Copy 5
RM L52I19

NACA RM L52I19

(2)

NACA

RESEARCH MEMORANDUM

EVALUATION OF END- AND RADIAL-BURNING SOLID FUELS IN RAM JETS MOUNTED IN A FREE JET AT MACH NUMBERS OF 2.0, 2.2, AND 2.3

By Walter A. Bartlett, Jr.

Langley Aeronautical Laboratory
Langley Field, Va.

NATIONAL ADVISORY COMMITTEE
FOR AERONAUTICS

WASHINGTON
November 25, 1952

NATIONAL ADVISORY COMMITTEE FOR AERONAUTICS

RESEARCH MEMORANDUM

EVALUATION OF END- AND RADIAL-BURNING SOLID FUELS IN RAM JETS MOUNTED IN A FREE JET AT MACH NUMBERS OF 2.0, 2.2, AND 2.3

By Walter A. Bartlett, Jr.

SUMMARY

Two types of solid fuels were evaluated in a $6\frac{1}{2}$- inch-diameter ramjet engine mounted in a free supersonic jet at Mach numbers of 2.0, 2.2, and 2.3. The fuel charges tested were an end-burning fuel, consisting of a solid cylinder $4\frac{1}{2}$ inches in diameter, and a radial-burning fuel in the form of a hollow cylinder, with an inside diameter of $4\frac{1}{4}$ inches and an outside diameter of $6\frac{1}{4}$ inches.

Both types of fuel charges gave essentially equal performance. The maximum values of air specific impulse obtainable at a fuel-air ratio of 0.15 are 140 seconds for the end-burning fuel charge (with suitable flame holder) and 145 seconds for the radial-burning fuel.

The peak values of impulse efficiency and combustion efficiency obtained were 83 and 61 percent, respectively, at a fuel-air ratio of 0.08 for both the radial-burning charges and the end-burning fuel with flame holders.

The need for flame-holder installation in the combustor with the end-burning fuel charges was established. Increases in air specific impulse of 30 seconds and in combustion efficiency of 30 percent were obtained with the flame holder installed over those obtained with the fuel charge alone.

The problem of combustion chamber burn-through was encountered even though the combustor shells were constructed of 0.093-inch Inconel. However, this was not experienced when the air specific impulse was less than 130 seconds.

INTRODUCTION

A solid-fuel ram jet is an intermediate power plant between the solid-fuel rocket, which possesses simplicity and reliability, and the liquid-fuel ram jet, which gives high performance with attendant complex fuel-metering devices. The use for the solid-fuel ram jet is found when the high thrust of a solid rocket is not required, yet it is desired to have a power plant that has good performance with the simplicity of a solid rocket. The use of solid fuels has been proposed and investigated by other agencies. A comprehensive review of available literature and data on this subject is presented in reference 1.

The apparent advantages of a solid-fuel ram jet have led the Pilotless Aircraft Research Division to institute an investigation to determine the performance of various types of fuel charges; first, in preliminary ground tests, and second, in flight tests. The data reported herein were obtained in the initial phase of this investigation in the preflight jet at Wallops Island, Va. (ref. 2).

The available theoretical and basic experimental work on two types of solid fuels (cylindrical, end-burning (ref. 3); and annular, radial-burning (ref. 4)) indicated that a high-energy solid fuel could be obtained which would possess good performance characteristics suitable for application to a solid-fuel ram jet. The most promising solid-fuel charges are made up of powdered light metals (aluminum, magnesium, or boron) with suitable binders and oxidizers molded into solid or annular cylindrical briquettes.

The available basic experimental data were, however, obtained in closed-duct tests with low values of air flow and static pressure. The object of this investigation was to obtain the characteristics of the fuels with the higher values of air flow and static pressure which would be encountered under actual flight conditions near sea level.

SYMBOLS

S_a	air specific impulse, lb of jet thrust/lb of air/sec
$\bar{S}_a$	average air specific impulse, $\frac{\int_0^t S_a \, dt}{t}$, sec
W_a	weight flow of air, lb/sec

[redacted]

$\bar{W}_f$	weight rate of fuel expenditure, the initial weight of the fuel charge divided by the burning time, lb/sec
$\bar{f}/a$	fuel-air ratio, $\frac{\bar{W}_f}{W_a}$ weight rate of fuel flow to weight rate of air flow
η_i	impulse efficiency, ratio of the experimental S_a to theoretical S_a at the same fuel-air ratio
η_c	combustion efficiency, ratio of the theoretical fuel-air ratio to the experimental fuel-air ratio to give the same value of S_a
p	static pressure, lb/sq in. abs
H	total pressure, lb/sq in. abs
t	time measured from ignition of the charge, sec
L^*	combustion-chamber volumetric parameter, in. (volume of the combustion chamber from the midpoint of fuel charge to nozzle exit, divided by the nozzle exit area)
C_{D_B}	burner drag coefficient
M	Mach number
A	area, sq ft.
γ	ratio of specific heats (1.4 for air, 1.2 for burning mixture)
T_{S_0}	free-stream stagnation temperature, $^{\circ}F$, abs

Subscripts:

0	free stream
1	entrance
2	diffuser
3	combustion-chamber entrance

[redacted]

4 combustion-chamber exit

5 nozzle exit

APPARATUS

The fuel-evaluation tests reported herein were conducted in the preflight-jet facility located at the Pilotless Aircraft Research Station, Wallops Island, Va. The tests were made in an 8-inch-diameter free jet at Mach numbers of 2.0, 2.2, and 2.3, with a free-stream stagnation temperature of 310° F (±10°) at standard sea-level static pressure.

Fuels

The solid fuels used in this investigation were of two distinct types: one, a radial-burning charge developed by the Continental Aviation and Engineering Corporation (ref. 4, fig. 1(a)), and the other, an end-burning charge developed by the Bureau of Mines (ref. 3(a)) fig. 1(b)). The compositions of both types of fuel charges were varied to give a range of fuel-air ratios for these tests. The features of construction of these two charges are described in the sections that follow.

Radial-burning fuel.- The radial-burning-fuel charge is made up of the following ingredients of fuel, oxidizer, and binder percentages:

	Early charges	Final charges
Fuel: magnesium, atomized	$85\frac{1}{2}$ to 93 percent	82 to $88\frac{1}{2}$ percent
Oxidizer: sodium nitrate	5 to $12\frac{1}{2}$ percent	$7\frac{1}{2}$ to 10 percent
Binder: {linseed oil / rubber cement}	2 percent	4 or 8 percent

The ingredients are thoroughly mixed and pressed into annular charges under a pressure of 4000 pounds per square inch. The charges are "cured" in an oven and then cemented in a hollow steel or magnesium cylinder. The fuel charges were of $4\frac{1}{4}$-inch inside diameter and $6\frac{1}{4}$-inch outside diameter. The fuel-charge weight was of the order of 16 pounds, and the charge length was approximately 19 inches. An annular igniter ring made up of barium nitrate, atomized magnesium, and Duco cement is

cemented to the upstream end of the fuel charge. Two match-type electric squibs attached to the igniter face and buried in a mixture of black powder and Duco cement are provided for ignition. The stoichiometric fuel-air ratio for the radial-burning fuel is given as 0.359 in reference 4.

End-burning fuel.- The end-burning fuel charge is made up of various mixtures of the following ingredients, with aluminum as the fuel either separately or collectively with magnesium or boron and added oxidizers:

Fuels	Aluminum, pyrotechnic - 37 to 60 percent Magnesium, 200 mesh - 0 to 30 percent Boron, amorphous - 10 percent
Oxidizers	Potassium nitrate - 14.3 to 25 percent Copper sulphate - 6.6 to 10 percent

The completed fuel charges had a range of fuel and oxidizer percentages as follows:

Fuel - 65 to 77 percent
Oxidizer - 35 to 23 percent

The ingredients are thoroughly mixed and pressed into a magnesium liner under a pressure of 4000 pounds per square inch. The liner is commercial extruded tubing of $4\frac{1}{2}$-inch outside diameter with a wall thickness of 0.093 inch. The fuel weight in a charge was of the order of 8 pounds. The fuel charge length was approximately 10 inches. A black-powder igniter ring is cemented to the downstream end of the charge, and is ignited with electric match squibs buried in the igniter. Reference 3(b), gives the stoichiometric fuel-air ratio as 0.392 for the end-burning fuel.

Ram-Jet Engines

Engine A.- A simple, normal-shock diffuser mounted on a 6.5-inch inside-diameter combustor shell was used in the preliminary evaluation tests on both types of fuel. A sketch of the engine and a photograph of the model mounted in the preflight jet are shown in figures 2(a) and 2(b). The products of combustion exhausted through a 6-inch-diameter sonic exit, which is shown in figure 2(a). The over-all length of the engine varied between 72.4 and 93.1 inches, depending upon the length of combustors used (fig. 2(a)). The area ratio of the diffuser was 0.253 based on the inlet capture area and the combustion-chamber area. The exit-nozzle contraction ratio was 0.853 based on the nozzle exit area and the combustion-chamber area. The inner body was used to support the end-burning charges and was removed for tests of the radial-burning

fuel. The inlet section, inner body, and exit nozzle were constructed of mild steel. The diffuser center section was made of aluminum, while the combustor shell was fabricated of 0.093-inch Inconel.

Engine B.- A Mach number 2.13 Ferri-type conical-shock inlet diffuser (fig. 2(c)) was used to test further the most promising charges after preliminary evaluation tests. The engine is 73.2 inches long and 6.6 inches in diameter. The area ratio of the combined supersonic and subsonic diffuser was 0.461. The exit-nozzle contraction ratio of the ram-jet engine was 0.853. Two diametrically opposite circular-arc airfoils with a thickness of $\frac{1}{2}$ inch and a chord of 3 inches fastened the inner body to the diffuser wall. The inner body and diffuser were constructed of aluminum. The exit nozzle was made of mild steel, and the combustor cans were constructed of 0.093-inch Inconel.

Flame holders or mixers.- Three distinct types of fuel-air mixers were used in some tests with the end-burning charge. Two types - the annular ring and the conical probe - were conceived and built by the NACA. The vane turbulator was furnished by the Bureau of Mines. The annular ring consisted of $\frac{1}{2}$-inch mild steel with $4\frac{1}{2}$-inch inside diameter and 6.5-inch outside diameter. This ring was mounted to the combustor shell 2 inches downstream of the charge (fig. 2(a)). The conical flame holders (fig. 3) consisted of cast aluminum cones with a 30° half angle and integral tripod legs for attaching to the combustor shell. The base diameters were $3\frac{1}{4}$ inches and $4\frac{1}{4}$ inches. The apex of the cone was located in the combustor 1 inch aft of the charge. The vane-type turbulator developed by the Bureau of Mines (ref. 3(b)) consisted of nine steel vanes, with a 3-inch chord, set at an angle of 30° to the normal direction of the air flow. The vanes were installed on the inner body immediately upstream of the fuel charge.

INSTRUMENTATION AND METHODS

Thrust measurements of the ram jet were obtained with high-frequency response strain-gage beams. Measurements of free-stream total and static pressures, diffuser exit static pressure, and nozzle base-pressure were obtained with electrical pressure pickups. The free-stream stagnation temperature was measured with an iron-constantan thermocouple. All of the above data were recorded on an oscillograph and time-correlated with a 10-cycle-per-second timer. The instruments used were accurate to

1 percent of the full-scale range. Time-correlated shadowgraph pictures were obtained of the inlet to provide positive information that:

(1) The normal shock was swallowed in engine A throughout the tests.

(2) Engine B did not buzz during combustion.

The air mass flow for engine A was determined from the known free-stream conditions, and the total geometric area of the inlet, as the normal shock was swallowed in the ram-jet diffuser at all times. The inlet contraction ratio in the diffuser of engine B was such that choking occurred in the minimum section of the diffuser to limit the free-stream tube area to a calibrated value of 0.102 square feet for use in the computation of air mass flow. This free-stream tube area was obtained in a similar manner to that described in reference 2.

The force measured on the thrust stand before ignition is made up of tare (external), internal, and exit-nozzle base drags. The tare drag was obtained by the method described in reference 2 and, together with the base-pressure drag, was added to thrust measurements obtained during combustion of the fuel for the computation of gross thrust. These gross-thrust measurements were converted to air specific impulse, S_a, for presentation in this report. The locations of stations used in obtaining and analyzing the data are shown in figures 2(a) and 2(c).

RESULTS AND DISCUSSION

The air specific impulse parameter S_a, developed in reference 5, is generally used to evaluate the performance of any fuel in an air-breathing propulsion engine such as a ram jet. This parameter is significant in that it is dependent upon the exit exhaust velocity and/or exhaust temperature (exhaust enthalpy). Hence an improvement in the heat release of the fuel per unit time by increasing either the combustion efficiency or by utilizing fuels with higher heating values will show directly as an increase in S_a.

Radial-Burning Fuel

The preliminary tests on the radial-burning fuel charges were conducted with fuels of the following compositions:

Magnesium - $85\frac{1}{2}$ to 93 percent

Linseed oil - 2 percent

Oxidizer - 5 to $12\frac{1}{2}$ percent

[redacted]

Engine A was used in this series of tests and the value of L^* was vari from 37.8 inches to 62 inches. The results of a representative test are shown as figure 4(a), with S_a presented as a time history. This test was conducted at $M = 2.2$, $W_a = 13.3$ lb/sec, and $L^* = 62$ inches, at standard sea-level static pressure, with a fuel composition of 93-percent magnesium, 5-percent oxidizer, and 2-percent linseed-oil binder. The ignition characteristics were considered satisfactory, with a value of $S_a \approx 155$ seconds obtained for approximately 1 second during combustion of the barium nitrate igniter ring. The S_a value then dropped to about 135 seconds and remained constant until $t = 2$ seconds. At this time burning and thrust became very erratic, until complete burnout occurred at 4.6 seconds. Motion pictures taken during these preliminary tests showed large pieces of burning and unburned magnesium being ejected from the ram-jet engine. Such an occurrence would explain the erratic thrust characteristics obtained during combustion of the radial-burning fuel charges.

A compilation of $\bar{S}_a$ obtained with the radial-burning fuel charges incorporating linseed-oil binders is presented in figure 4(b) as a function of fuel-air ratio, $\bar{f}/a$. The weight rate of fuel expenditure, used in computing $\bar{f}/a$, was obtained by dividing the initial weight of the fuel charge by the burning time. Included are curves of theoretical S_a and experimental S_a obtained from reference 4. The $\bar{S}_a$ values obtained in this investigation varied from 33 to 45 seconds lower than those presented in reference 4 over the range of $\bar{f}/a = 0.15$ to 0.23.

The combustion-chamber volumetric parameter L^* was varied from 37.8 inches to 62 inches, with fuels having 5 or $7\frac{1}{2}$ percent oxidizer to determine the L^* effect. Figure 4(c) presents $\bar{S}_a$ plotted against L^*, and demonstrates no noticeable increase in $\bar{S}_a$ with increasing L^*. Data presented in reference 4 indicated a slight improvement in combustion parameters with increases in the L^* parameter over the range of L^* covered by these tests.

Combustion efficiencies η_c and impulse efficiencies η_i computed from data obtained with the linseed-oil binder radial-burning fuels are presented in figure 4(d) as a function of $\bar{f}/a$. Values of η_c and η_i of approximately 0.30 and 0.65 were obtained over the $\bar{f}/a$ range of 0.15 to 0.23.

A study of the motion pictures, together with visual observation of tests of the preliminary radial-burning charges, gave evidence that the fuel charges were breaking up. The data presented in reference 4 were obtained with air mass flows and diffuser static pressures of the order of 10 pounds per second and 35 pounds per square inch absolute, with no

[redacted]

evidence of physical deterioration of the fuel charge. Evidently the combination of higher air mass flows (13.3 lb/sec) and static pressures (70 lb/sq in., absolute) caused failure of the fuel charges so that closer agreement with the data of reference 4 was prevented.

At the conclusion of this series of tests, Continental Aviation and Engineering Corporation reported that the substitution of a rubber cement binder for linseed oil would raise the compressive strength of the fuel strands from 170 psi to 1190 psi, as well as considerably reduce erosion of the charge due to air flow. Accordingly, in the next series of tests, these new type fuels were specified. These charges had the following compositions:

Charge Designation	Magnesium	Oxidizer	Binder (rubber cement)
A	$88\frac{1}{2}$ percent	$7\frac{1}{2}$ percent	4 percent
B	$84\frac{1}{2}$ percent	$7\frac{1}{2}$ percent	8 percent
C	82 percent	10 percent	8 percent

The test results obtained with these charges are shown as figure 5(a). Fuel charges A and B were tested in engine A, with $M = 2.2$, $W_a \approx 13.3$ pounds per second, and $L^* = 37.8$ inches. The thrust buildup occurred in the short time of 0.25 second with both charges. Greatly improved burning characteristics were obtained, as indicated by the increased burning time, the more uniform thrust output, and the absence of fuel-charge breakup during combustion. Approximately 5 seconds after ignition, combustor-can failure occurred with charge A installed. When the 0.093-inch sheet Inconel combustor burned off immediately downstream of the fuel charge, a sudden drop in S_a occurred, together with some erratic burning. When the rubber binder was increased to 8 percent in charge B, the burning time increased to 13.25 seconds, with instantaneous values of S_a somewhat lower than those obtained with charge A throughout the duration of the test. Increases in rubber-cement binder decreased the burning rate, with attendant decreases in $\bar{f}/a$ and S_a.

Due to the promising results obtained with fuel charges A and B which incorporated a rubber-cement binder, strand C was further tested in engine B. This charge was tailored to give a value of S_a between those values obtained with the fuels made up of 4 and 8 percent rubber cement binder incorporating $7\frac{1}{2}$ percent sodium nitrate oxidizer. This test was conducted at $M = 2.0$, $W_a = 19.1$ pounds per second, and $L^* = 43$ inches. The time history of S_a is presented in figure 5(a). At the time of 4.8 seconds after ignition, the 0.093-inch Inconel

combustor shell burned off downstream of the fuel charge; however, the fuel charge performance was very satisfactory.

A compilation of $\bar{S}_a$, as obtained from tests of the rubber-binder fuel charges, is presented in figure 5(b) as a function of $\bar{f}/a$. It is noted that the values of $\bar{S}_a$ given for charges A and C were computed assuming that no thrust drop-off occurred with combustor-shell failure, but that the value of S_a obtained immediately before failure held constant until burnout of the fuel charge. Included are curves of theoretical S_a, and experimental S_a, as obtained from tests of annular magnesium solid-fuel charges with $L^* = 62$ inches, as reported in reference 4. With the fuel breakup problem eliminated, good agreement in performance is noted between results of tests reported herein and the results of reference 4. The experimental curve of S_a from reference 4 was obtained from tests of fuel charges incorporating linseed-oil binders at low air mass flows and combustion-chamber pressures. Under these conditions there was no apparent fuel breakup. The tailoring of a fuel charge to meet a specific missile booster requirement is deemed possible as a result of the correlation of $\bar{S}_a$ with $\bar{f}/a$, when oxidizer and rubber-binder percentages are varied. The problem of combustor shell failure, however, must be corrected before the full potentialities of the solid-fuel ram jet may be utilized.

Combustion efficiencies η_c and impulse efficiencies η_i calculated from performance data obtained with rubber-cement binder annular charges are presented in figure 5(c). Maximum values of $\eta_c = 0.61$ and $\eta_i = 0.83$ were obtained at $\bar{f}/a = 0.08$.

The ratios of diffuser static pressure p_2 to free-stream total pressure H_0 calculated from data obtained during evaluation of the $7\frac{1}{2}$ percent sodium nitrate, 4-percent (charge A), and 8-percent (charge B) rubber-binder fuel charges, are presented as time histories in figure 6. These data were obtained in engine A with $M = 2.2$, $W_a \approx 13.3$ pounds per second, and $H_0 = 151 \pm 2$ pounds per square inch, absolute. Peak values of p_2/H_0 of approximately 0.6 were obtained with both charges at ignition (during combustion of the barium nitrate igniter ring). The inlet of this engine was sized to allow operation of the engine over a wide range of fuel-air ratios without spillage; hence, low values of p_2/H_0 were obtained at the relatively low fuel-air ratios covered in this paper.

A summary and comparison of the important fuel-evaluation parameters (S_a, η_i, and η_c) presented in this report from tests of annular

charges and from data of reference 4 are given in figure 7 as functions of $\bar{f}/a$. Values of $\bar{S}_a$ obtained with rubber-binder charges (fig. 7(a)) were in good agreement with those of reference 4, and were approximately 27 seconds higher, at a comparable fuel-air ratio, than those obtained with charges incorporating a linseed-oil binder. Increases in η_i of 12 to 18 percent (fig. 7(b)) were obtained with rubber binders over those of linseed-oil binders. The peak value of $\bar{\eta}_i = 0.83$ with the rubber binder occurred at $\bar{f}/a = 0.08$, while the data of reference 4 give a peak $\eta_i = 0.88$, occurring at $f/a = 0.25$. Data on η_c are presented in figure 7(c). An increase in η_c of approximately 0.30 was realized with the rubber-cement binder incorporated in the charge rather than linseed oil. Peak values of $\eta_c = 61$ percent were obtained with the rubber-binder charges ($L^* = 43$ in.) and with those calculated from data of reference 4. ($L^* = 62$ in.) The peak value was obtained at $\bar{f}/a = 0.08$ for this series of tests, while that in reference 4 occurred at $f/a = 0.15$. There is reasonably good agreement between the peak values of η_i and η_c obtained in these tests and those reported in reference 4. The peaks occur, however, at widely different fuel-air ratios. The reason for this difference is not apparent.

End-Burning Fuel

The development tests of the Bureau of Mines on end-burning fuels (ref. 3(a)) were conducted at low values of air mass flow (4 lb/sec) and diffuser static pressure (30 lb/sq in. abs). A serious problem in fuel breakup occurred when the first group of end-burning charges was tested in the preflight-jet facility at higher values of air mass flow and diffuser static pressure. The results of a test of one of the first series of fuel charges in which fuel breakup was experienced are presented in figure 8(a) with S_a plotted against burning time. The test conditions were: $M = 2.2$, $W_a = 13.3$ pounds per second, and $L^* = 67$ inches. This test, as well as the other initial tests, was conducted in engine A. The diffuser static pressure was of the order of 65 pounds per square inch absolute. The three distinct peaks of S_a (fig. 8(a)) occurred when large sections of fuel broke away from the charge and caused accelerated burning with attendant increases in S_a. Visual observation and motion pictures showed large pieces of burning fuel being expelled from the combustion chamber at these instances. A compilation of $\bar{S}_a$ obtained from data of the initial series of charges is presented in figure 8(b) as a function of $\bar{f}/a$. Values from the faired curve show $\bar{S}_a$ varying from 87 seconds at $\bar{f}/a = 0.099$ to 100 seconds at $\bar{f}/a = 0.18$. Rapid and favorable charge ignition characteristics were obtained during this series of tests. The theoretical S_a curve for aluminum-type fuel presented in figure 8(b) was obtained from reference 3(c).

[redacted]

Visual observation, together with motion-picture studies, showed that most of the combustion occurred downstream of the ram-jet exit, indicative of improper mixing of the fuel and air in the combustion chamber in addition to fuel breakup. In order to eliminate this external burning, two simple fuel-air mixers - an annular ring and a conical probe - were developed and tested by the NACA (figs. 2(a) and 3). The results obtained with either flame holder installed in the combustor in conjunction with the end-burning charges are shown as individual points of $\bar{S}_a$ on figure 8(b). With flame-holders installed the fuel performance was slightly improved, and motion-picture studies demonstrated a marked reduction in external burning. However, fuel breakup precluded successful evaluation of the effect of fuel-air mixers on fuel performance.

Values of η_c and η_i computed from data obtained in the initial series of end-burning fuel-charge tests are shown in figure 8(c) as functions of $\bar{f}/a$. These data include three values of η_i and η_c computed from data with the flame holders installed. Combustion efficiency η_c of the order of 18 percent and impulse efficiency η_i of the order of 50 percent were obtained with no flame holders installed. With the addition of flame holders to the burner configuration, slightly higher values were obtained.

As a result of the initial series of tests, the Bureau of Mines recognized that problems in fuel breakup and improper mixing of fuel and air resulted in the poor performance of the end-burning fuel. A new molding technique for the end-burning charge was developed and reported in reference 3(b). It was believed that this technique would eliminate the fuel breakup problem. The NACA annular ring was adapted by them as a standard flame holder for their fuel development work and resulted in greatly improved fuel performance. The fuel charges formed by the process described in reference 3(b) were next furnished the NACA for fuel-evaluation tests.

Representative results of S_a computed from test data are presented in figure 9(a) as time histories obtained with the end-burning fuel without mixing devices, with the annular ring installed, and with the annular ring plus the Bureau of Mines vaned turbulator. These tests were conducted at $M = 2.3$, $W_a \approx 13.9$ pounds per second, and $L^* = 43$ inches in engine A.

The fuel composition was:

55 percent aluminum, pyrotechnic
10 percent boron
25 percent potassium nitrate
10 percent copper sulphate

[redacted]

The pertinent results of these tests, together with the flame-holder configuration used, are summarized in the following table:

Flame holder		$\bar{S}_a$, sec	Burning time, sec
Ring	Vanes		
		87	9.4
X		110	8.4
X	X	110	7.6

The combustor shell burned through about 6 seconds after ignition with the annular ring and vanes installed in the combustion chamber; however, if it is assumed that the combustor did not fail, the $\bar{S}_a$ would increase to approximately 112 seconds, but the total impulse would still be lower than that obtained with the annular ring alone.

The fuel charges evaluated in this series of tests did not have as favorable ignition characteristics as did the initial end-burning charges. This problem might be alleviated with the installation of an ignitor having a higher heat of combustion than black powder. The new molding technique produced charges of greater strength, with the resultant elimination of fuel breakup. The burning times were greatly increased, the combustion process was smoother, and the need for a flame holder was established during tests with these fuel charges.

The values of $\bar{S}_a$ computed from test data of the several fuel charges are presented in figure 9(b). Results are presented with flame holder and without flame holder installed in the combustor. Theoretical and experimental results obtained from reference 3(c) are included. The excellent agreement between the results reported herein with flame-holder installation and those of reference 3(c) is noted. For this reason, the experimental data from reference 3(c) was used in calculations of η_i and η_c over the fuel-air ratio range of 0.125 to 0.180. Incorporation of flame holders in the combustion-chamber configuration increased $\bar{S}_a$ 27 to 30 seconds over those obtained without the flame holders installed in the combustor.

A comparison of the impulse efficiencies η_i computed from test data with and without flame holders installed is presented in figure 9(c). A peak value of $\eta_i = 0.83$ was realized with the flame-holder configuration, as against $\eta_i = 0.68$ without the flame holder.

The combustion efficiencies η_c as functions $\bar{f}/a$, obtained from data for the fuel charges tested with and without flame holders installed,

[redacted]

are presented in figure 9(d). Flame-holder installation increased η_c by the approximate amount of 0.30 throughout the experimental range of $\bar{f}/a = 0.06$ to 0.17.

The ratio of diffuser static pressure p_2 to free-stream total pressure H_0 is plotted as a time history in figure 10 for the burner configuration without flame holder, with annular ring, and with the annular ring plus vane turbulator. These data correspond with S_a time histories of figure 9(a). The drop-off in p_2/H_0 at the time of 5 seconds resulted from combustion shell failure for the ring-plus-vane turbulator configuration. The value of H_0 for these runs was 182 ±2 pounds per square inch absolute.

COMPARISON OF END- AND RADIAL-BURNING FUELS

The results of evaluation tests of the end-burning fuel charges (molded to prevent fuel breakup), in conjunction with flame holders installed in the burner, are markedly similar to those results obtained with the rubber-cement binder radial-burning fuel charges. These two sets of data are compared in figures 11 and 12 by using $\bar{S}_a$, η_i, and η_c for this purpose. Experimental data from reference 3(c), for the end-burning fuel is included in the figures above—the fuel-air ratio of 0.125. The theoretical values of S_a for end-burning fuels (ref. 3(c)) and radial-burning fuels (ref. 4) are included in figure 11. Slightly higher values of $\bar{S}_a$ were obtained with the radial-burning charges over the range of $\bar{f}/a$ (0.064 to 0.150) covered by these tests. If fuel charges with faster burning rates were tested, the maximum values of $\bar{f}/a$ (0.150 for the radial-burning, and 0.125 for the end-burning fuels) obtained in these tests would have increased proportionately.

Peak values of $\eta_i = 0.83$ were obtained with both types of charges at an approximate $\bar{f}/a = 0.08$. Peak values of $\eta_c = 0.61$ were realized for both types of fuel at approximately $\bar{f}/a = 0.08$.

The burner drag is an important parameter to use in the evaluation of various burner configurations. It is desirable to choose that configuration which gives the highest thrust with the least amount of drag. Values of burner drag coefficient C_{D_B} calculated for both the radial-burning and end-burning charges with and without flame holders are presented in figure 13 as functions of S_a. The following equation was used

$$C_{D_B} = \frac{p_3 A_3 \left(1 + \gamma_3 M_3^2\right) - p_4 A_4 \left(1 + \gamma_4 M_4^2\right)}{\frac{\gamma_2}{2} p_2 A_2 M_2^2}$$

[redacted]

with the assumption that no total-pressure loss occurred from station 2 to 3, and from station 4 to 5 in equating the change in momentum between stations 3 and 4. The burner drag coefficients are to be used as qualitative values only for purposes of comparison. The values of C_{D_B} presented for the end-burning fuel charges are for the three different burner configurations tested, and for which data on S_a, η_i, and η_c were presented in figure 9. At a value of S_a = 110 seconds, C_{D_B} = 3.4 for the end-burning fuel annular-ring burner configuration and increases to a value of 4.6 when the vaned turbulator is added to the combustor. It is noted that burner drag decreases with increases of S_a for the three end-burning-charge burner configurations. The values of C_{D_B} for the radial-burning fuel were computed from test data obtained during combustion of the $88\frac{1}{2}$- percent magnesium, $7\frac{1}{2}$- percent sodium nitrate, and 4-percent rubber cement charge. The performance parameters for this charge were presented in figure 5. Note the steady decrease in C_{D_B} with burning time as the restricted area in the combustor decreases during progressive burning of the charge.

CONCLUDING REMARKS

The important results obtained in free-jet tests of ram jets powered by end-burning and radial-burning solid-type fuels can be summarized as follows:

1. The problem of fuel breakup experienced during initial tests of both types of charges was not apparent when tests were conducted on the charges formed with recently developed molding techniques which resulted in charges of improved mechanical properties.

2. The need for a flame-holder installation in the combustor with the end-burning fuel charges was established. Increases in air specific impulse of 30 seconds and in combustion efficiency of 30 percent were obtained with the flame holder installed over those obtained with the fuel charge alone.

3. The maximum values of air specific impulse obtainable at a fuel-air ratio of 0.15 are 140 seconds for the end-burning fuel equipped with flame holders and 145 seconds for the rubber-cement binder radial-burning charge. The maximum value of fuel-air ratio obtained in these tests was limited by the burning rate of the fuel charges.

4. Peak impulse efficiencies of 83 percent were obtained with both the rubber-cement binder radial-burning charges and end-burning charges equipped with flame holders at an approximate fuel-air ratio of 0.08.

[redacted]

5. Both the radial-burning charges - with rubber-cement binder - and the end-burning charges plus flame holders gave peak combustion efficiencies of 61 percent at an approximate fuel-air ratio of 0.08.

6. Combustor shell burn-through was experienced during combustion of both types of charges when the value of air specific impulse was equal to or greater than 130 seconds.

7. At the same value of air specific impulse, the burner-drag coefficient was approximately 25 percent higher when the vaned turbulator was added to the annular-ring flame-holder configuration in the end-burning fuel-strand tests.

Langley Aeronautical Laboratory
National Advisory Committee for Aeronautics
Langley Field, Va.

REFERENCES

1. Olson, Walter T., and Gibbons, Louis C.: Status of Combustion Research on High-Energy Fuels for Ram Jets. NACA RM E51D23, 1951.

2. Faget, Maxime A., Watson, Raymond S., and Bartlett, Walter A., Jr.: Free-Jet Tests of a 6.5-Inch-Diameter Ram-Jet Engine at Mach Numbers of 1.81 and 2.00. NACA RM L50L06, 1951.

3. Damon, Glenn H., and Herickes, Joseph A.: Combustion of Solid Fuels for Ram Jets. Bur. Mines (Pittsburgh).

   (a) Prog. Rep. No. 19 (Proj. NAer 01045), Oct. 1 to Dec. 31, 1950.
   (b) Prog. Rep. No. 21 (Proj. NAer 01045), April 1 to June 30, 1951.
   (c) Prog. Rep. No. 22 (Proj. NAer 01206), July 1 to Sept. 30, 1951.

4. Squiers, John C.: Summary Report on Solid Fuel Ram Jet Development. Continental Aviation and Engineering Corp., July 30, 1950 (Air Forces Contract W-33-038-ac-13371).

5. Rudnick, Philip: Momentum Relations in Propulsive Ducts. Jour. of Aero. Sci., vol. 14, no. 9, Sept. 1947, pp. 540-544.

[redacted]

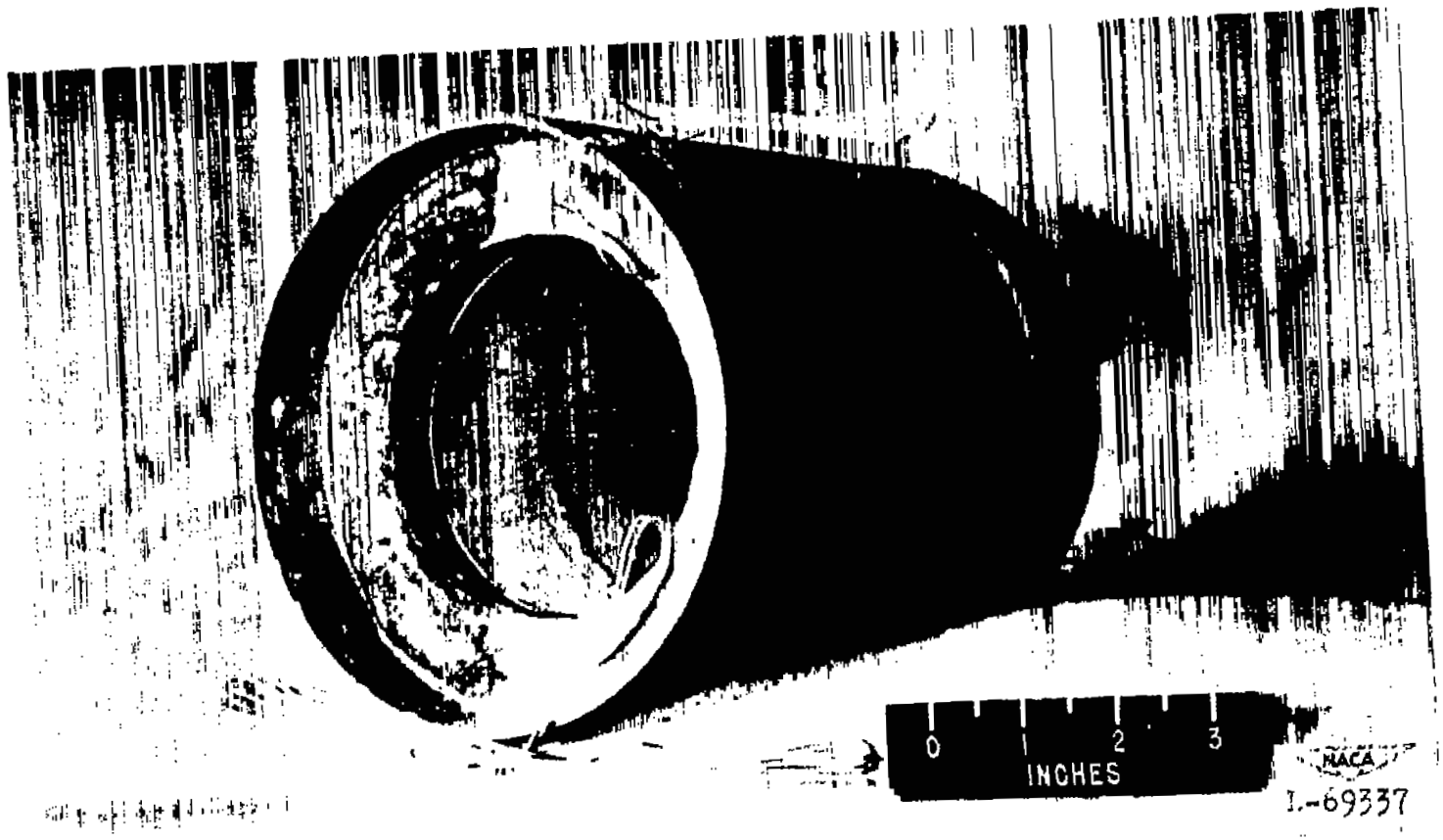

(a) The upstream end of radial-burning fuel charge showing igniter leads and black powder mixture mounted on the igniter ring.

Figure 1.- Photographs of the radial-burning and end-burning solid-fuel charges.

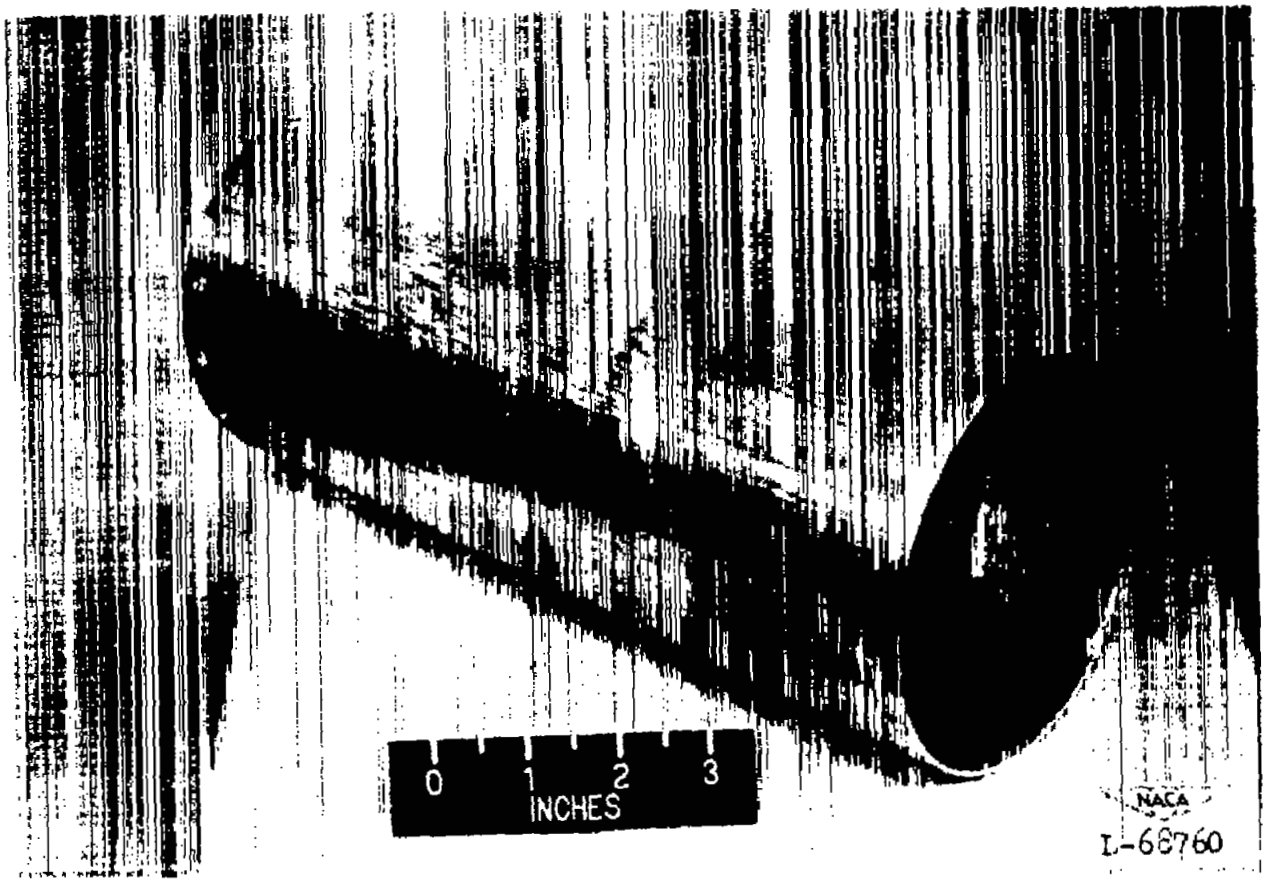

(b) The end-burning fuel charge showing black powder mixture molded to downstream end.

Figure 1.- Concluded.

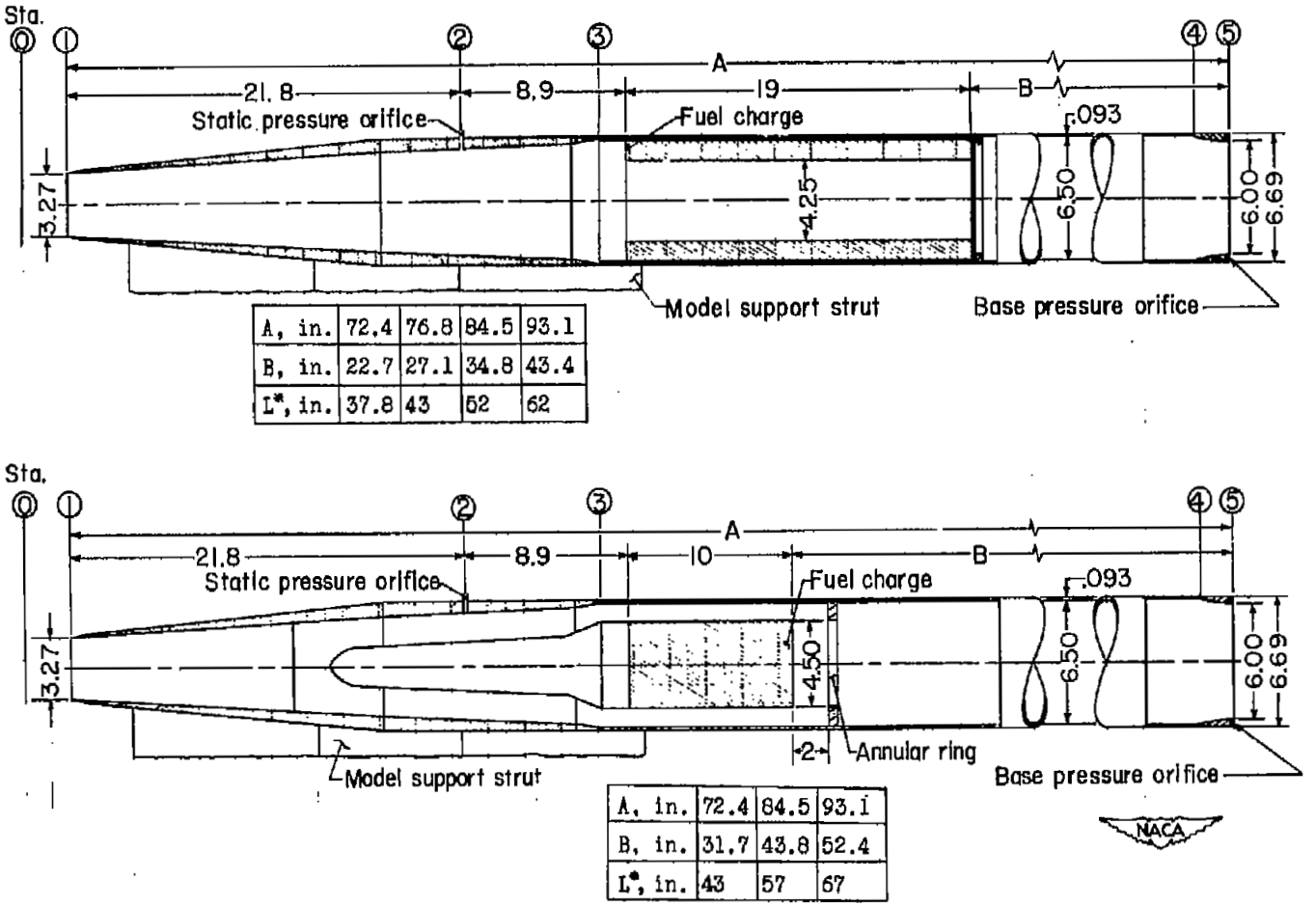

A, in.	72.4	76.8	84.5	93.1
B, in.	22.7	27.1	34.8	43.4
L*, in.	37.8	43	52	62

A, in.	72.4	84.5	93.1
B, in.	31.7	43.8	52.4
L*, in.	43	57	67

(a) Ram-jet engine A showing principal dimensions and installation of the end-burning (lower view) and radial-burning (upper view) solid fuels. (All dimensions are in inches.)

Figure 2.- The ram-jet engines used for the solid-fuel performance tests.

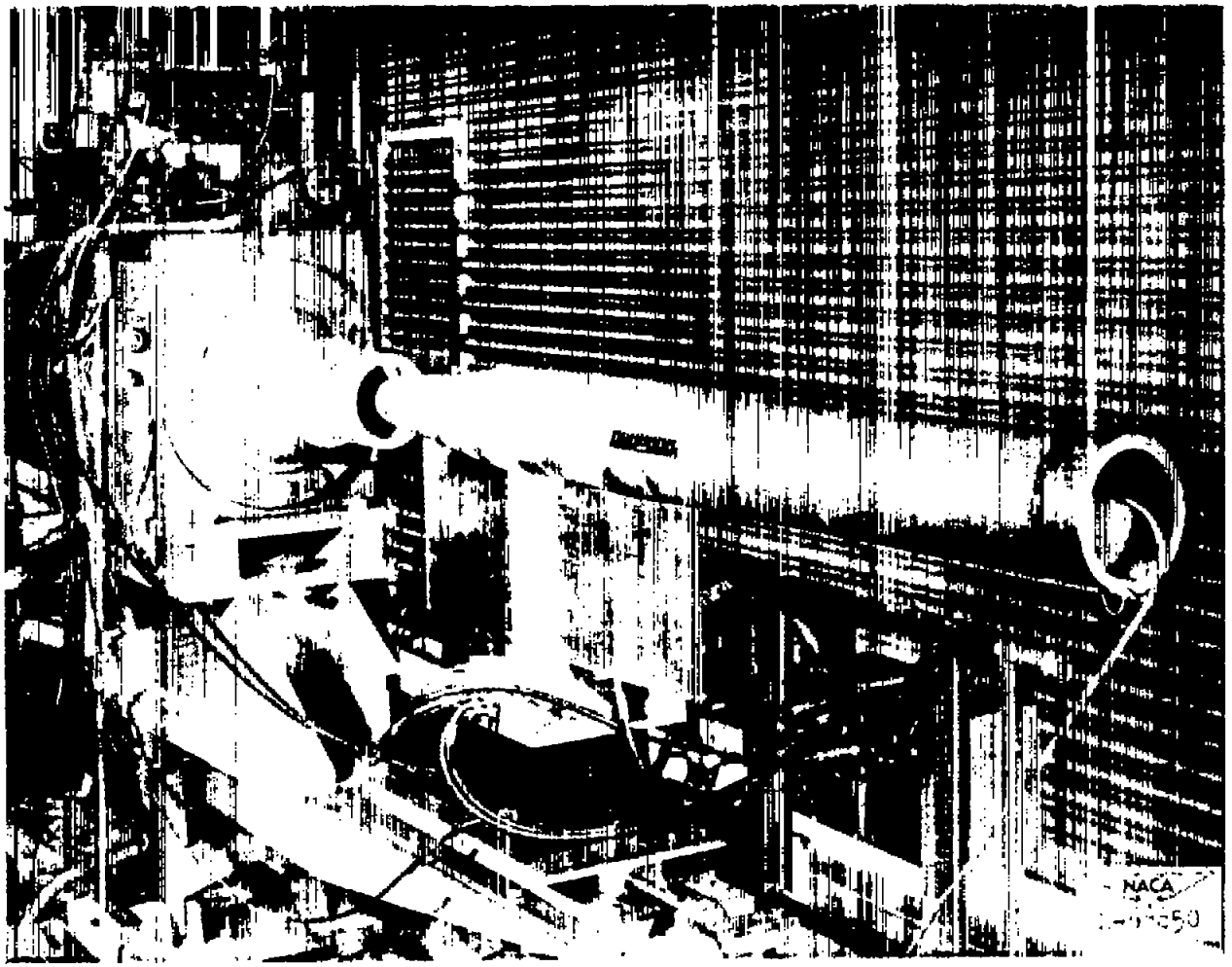

(b) Ram-jet engine A mounted in the preflight jet.

Figure 2.- Continued.

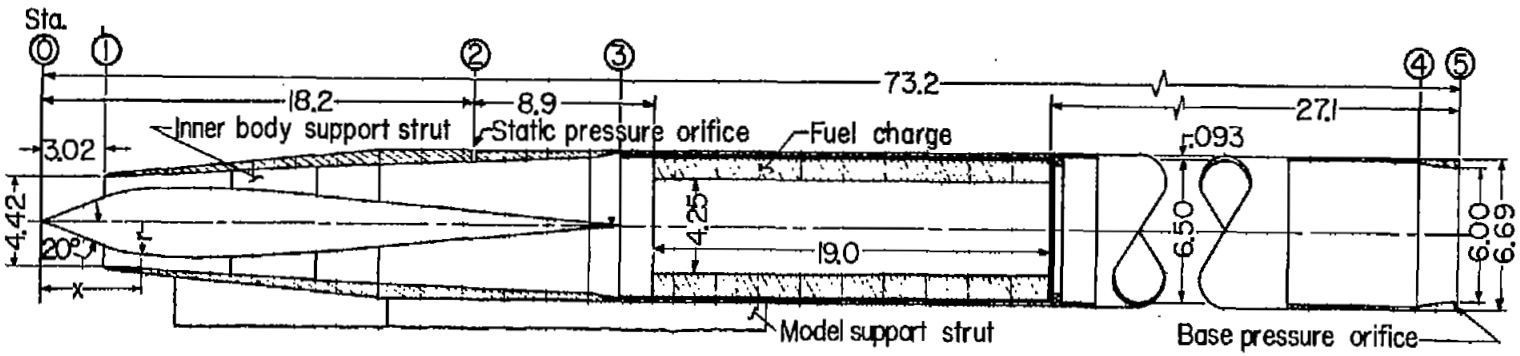

Stations where pressure was measured and/or data were analyzed

0	Free stream
1	Entrance
2	Diffuser
3	Combustion-chamber entrance
4	Combustion-chamber exit
5	Sonic exit

Inner-body ordinates

x, in.	0	3.500	3.600	3.700	3.800	3.900	4.000	4.120	4.620	5.120	5.620	6.120
r, in.	0	1.272	1.316	1.338	1.356	1.376	1.390	1.400	1.438	1.468	1.490	1.504
x, in.	6.620	7.000	8.000	9.000	10.000	11.000	12.000	13.000	14.000	25.600		
r, in.	1.510	1.510	1.500	1.480	1.440	1.380	1.310	1.240	1.170	0		

(c) Ram-jet engine B with radial-burning charge installed showing principal dimensions and stations used in data presentation. (All dimensions are in inches.)

Figure 2.- Concluded.

Figure 3.- The conical flame holders used in conjunction with evaluation of the end-burning fuels in ram-jet engine A.

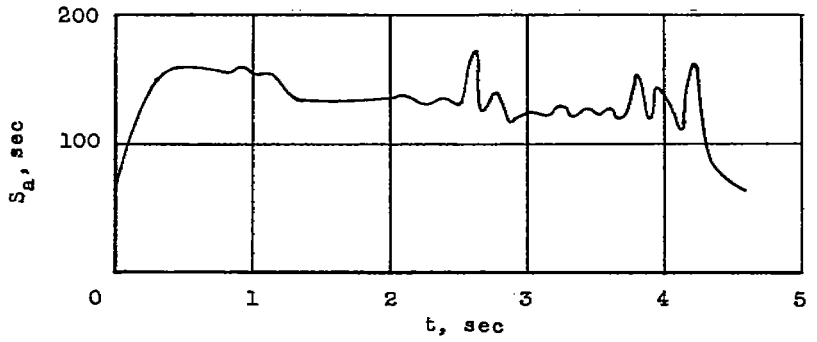

(a) Time history of specific air impulse for a representative test demonstrating erratic burning. L* = 62 inches; fuel: 93 percent magnesium, 5 percent sodium nitrate, and 2 percent linseed oil.

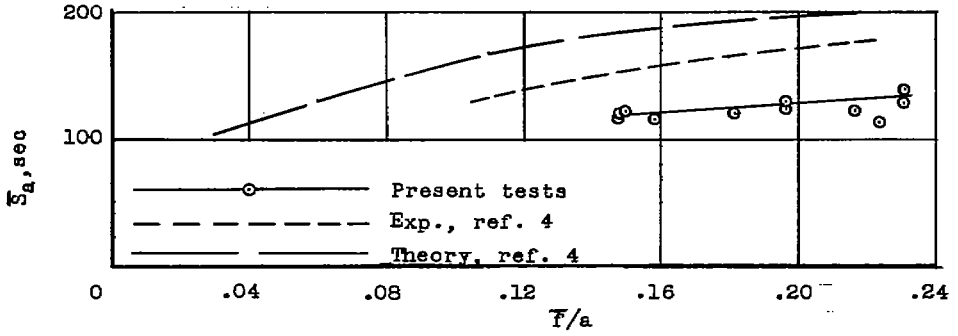

(b) The average air specific impulses as a function of fuel-air ratio.

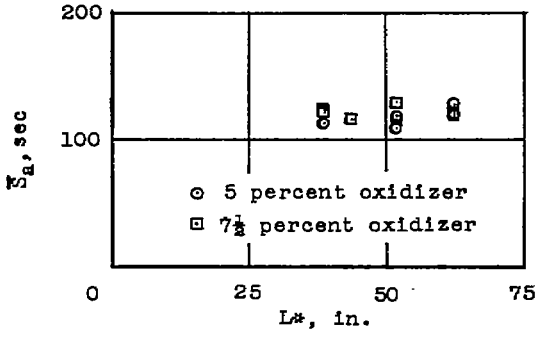

(c) The effect of L* on the average air specific impulse.

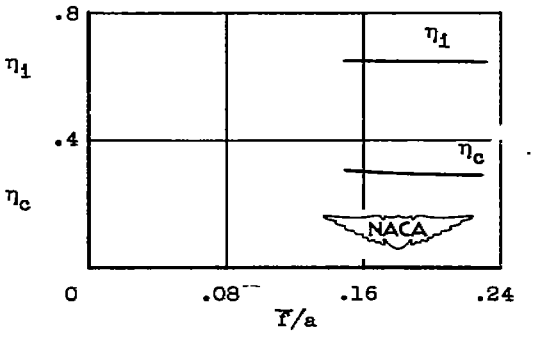

(d) The relationship of impulse and combustion efficiencies to fuel-air ratio.

Figure 4.- Performance of radial-burning fuels with linseed-oil binders in engine A. $W_a \approx 13.3$ pounds per second; M = 2.2; $L^* = 37.8$ inches to 62 inches; $T_{S_0} = 310^\circ$ F.

[redacted]

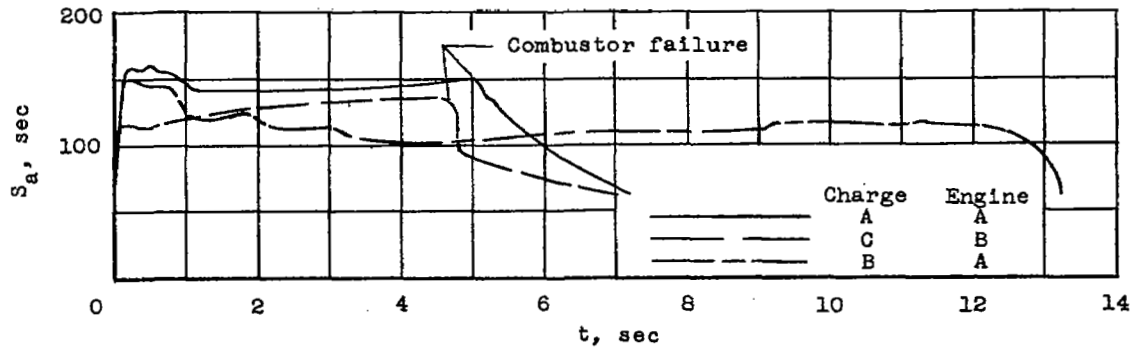

(a) Time histories of specific air impulse.

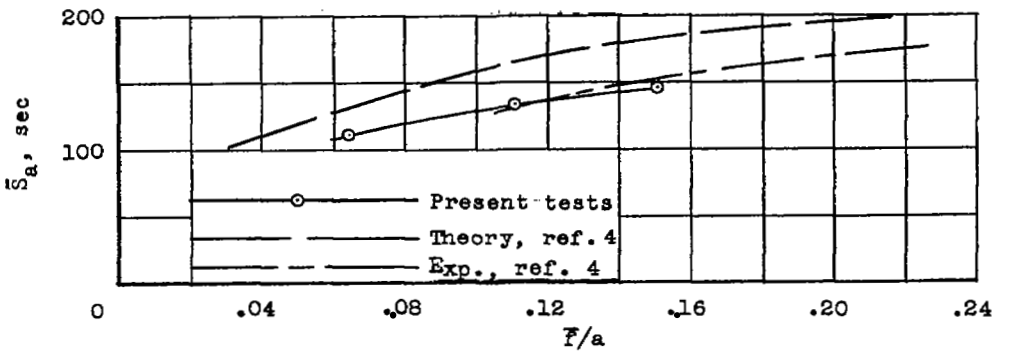

(b) The average air specific impulses as a function of fuel-air ratio.

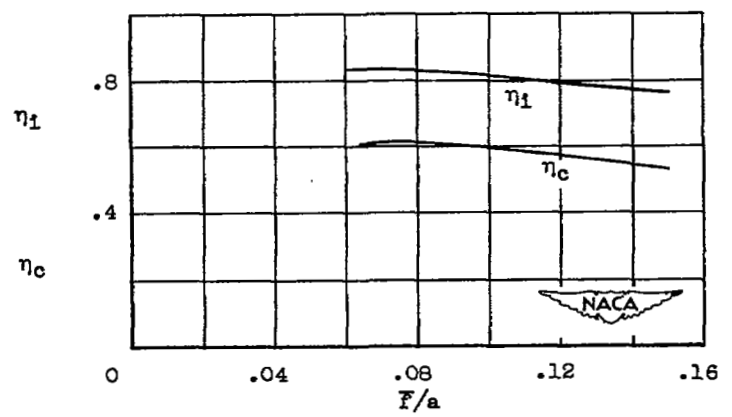

(c) The relationship of impulse and combustion efficiencies to fuel-air ratio.

Figure 5.- Performance of radial-burning fuels with rubber-cement binder in engines A and B. L^* = 37.8 inches; T_{S_0} = 310° F. Engine A: $W_a \approx 13.3$ pounds per second, M = 2.2. Engine B: $W_a \approx 19.1$ pounds per second, M = 2.0.

[redacted]

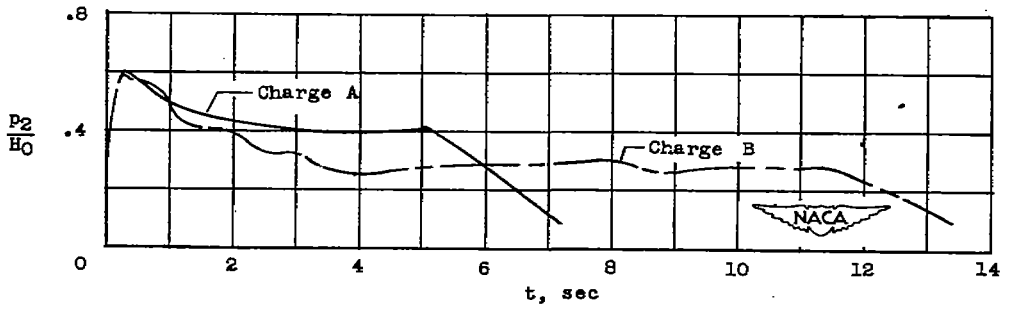

Figure 6.- Time histories of diffuser static pressure coefficients obtained with radial-burning rubber-base fuel strands in engine A. L^* = 37.8 inches; T_{S_0} = 310° F; M = 2.2; $W_a \approx 13.3$ pounds per second; H_0 = 151 ±2 pounds per square inch absolute.

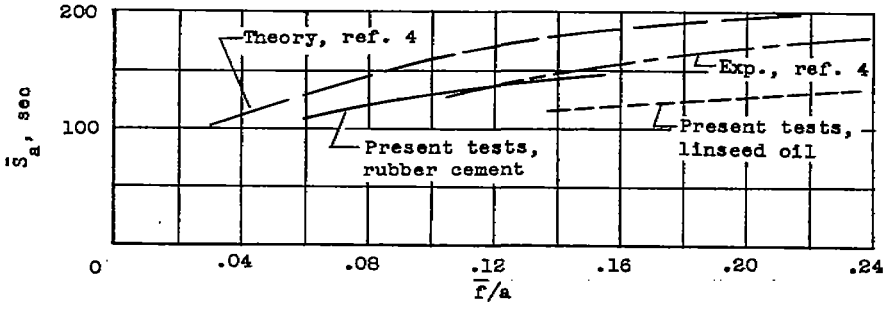

(a) The average air specific impulses as a function of fuel-air ratio.

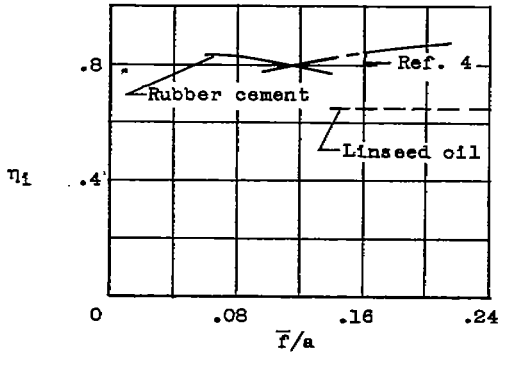

(b) The relationship of impulse efficiency to fuel-air ratio.

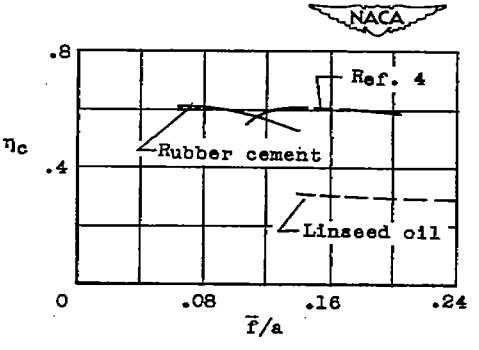

(c) The relationship of combustion efficiency to fuel-air ratio.

Figure 7.- Comparison of the performance of radial-burning fuels incorporating either linseed-oil or rubber-cement binders.

[redacted]

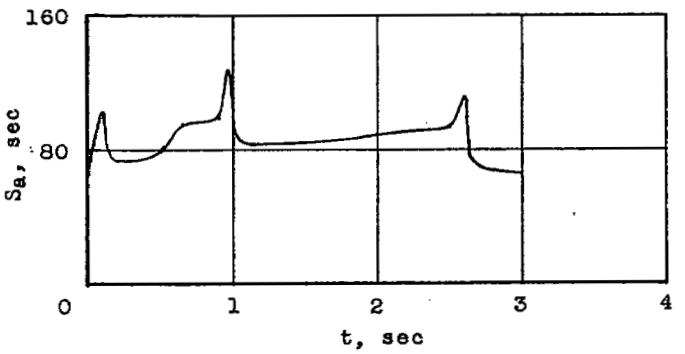

(a) Time history of air specific impulse for a representative test demonstrating erratic burning. L* = 67 inches; without flame holders.

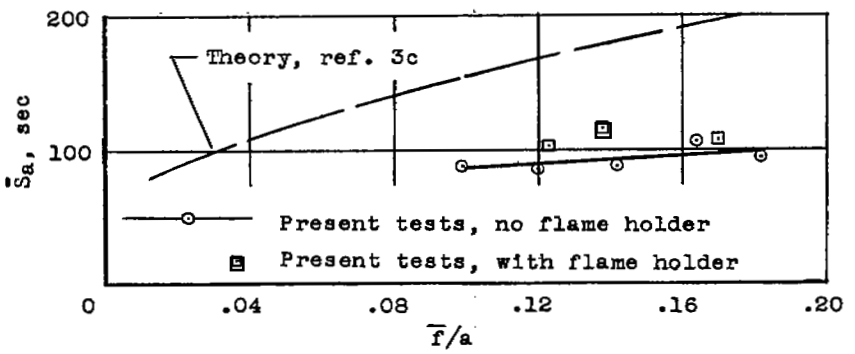

(b) The average air specific impulse as a function of fuel-air ratio, with and without flame holders installed.

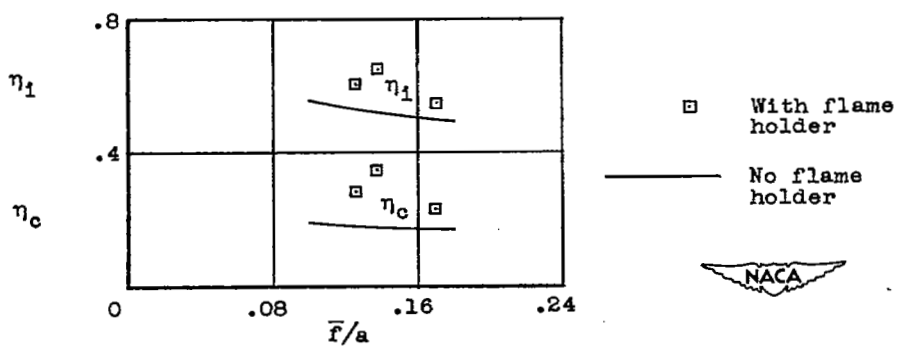

(c) The relationship of impulse and combustion efficiencies to fuel-air ratio with and without flame holders installed.

Figure 8.- Performance of the first series of end-burning fuel charges in engine A. $W_a \approx 13.3$ pounds per second; M = 2.2; L* = 57 and 67 inches; $T_{S_O} = 310^\circ$ F.

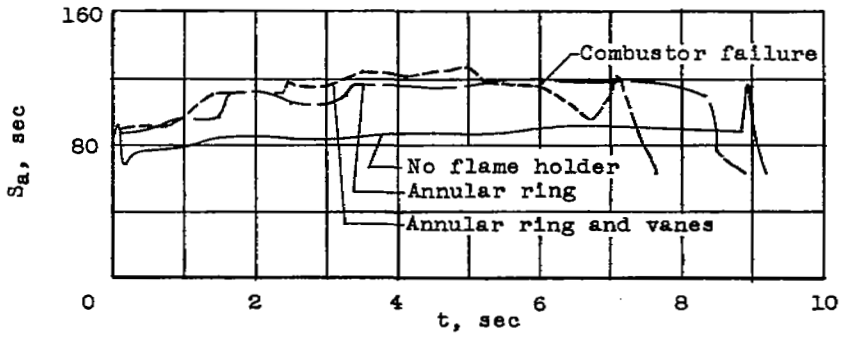

(a) Time histories of air specific impulse for representative tests of one fuel composition as effected by varying flame-holder configuration.

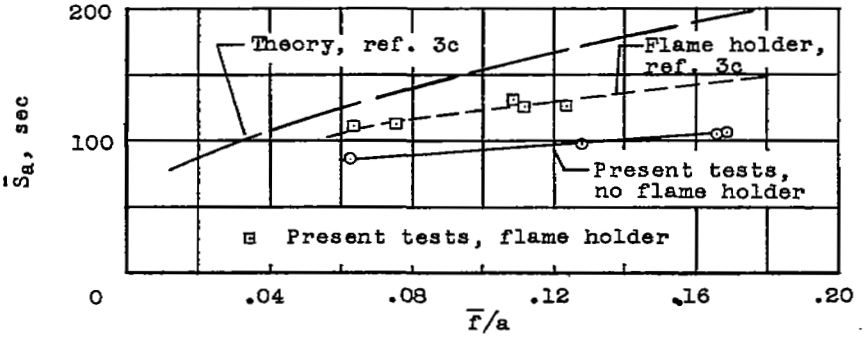

(b) The average air specific impulses as a function of fuel-air ratio, with and without flame holders installed.

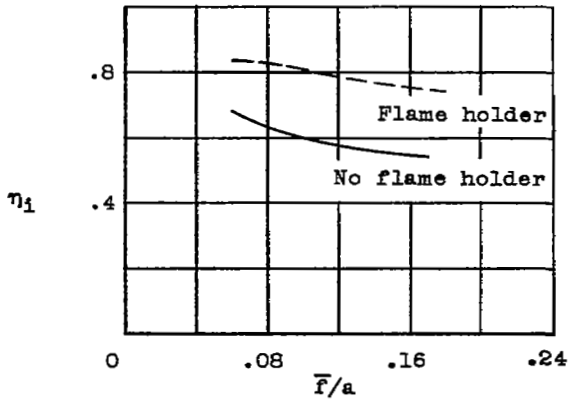

(c) The effect of flame-holder installation on impulse efficiency.

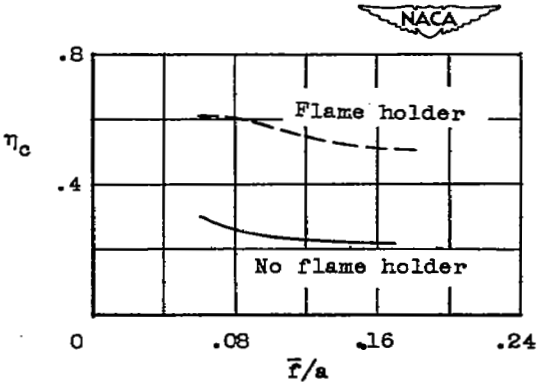

(d) The effect of flame-holder installation on combustion efficiency.

Figure 9.- Performance of the second series of end-burning fuels in engine A, with and without flame holders. $M = 2.3$; $W_a \approx 13.9$ pounds per second; $L^* = 43$ inches.

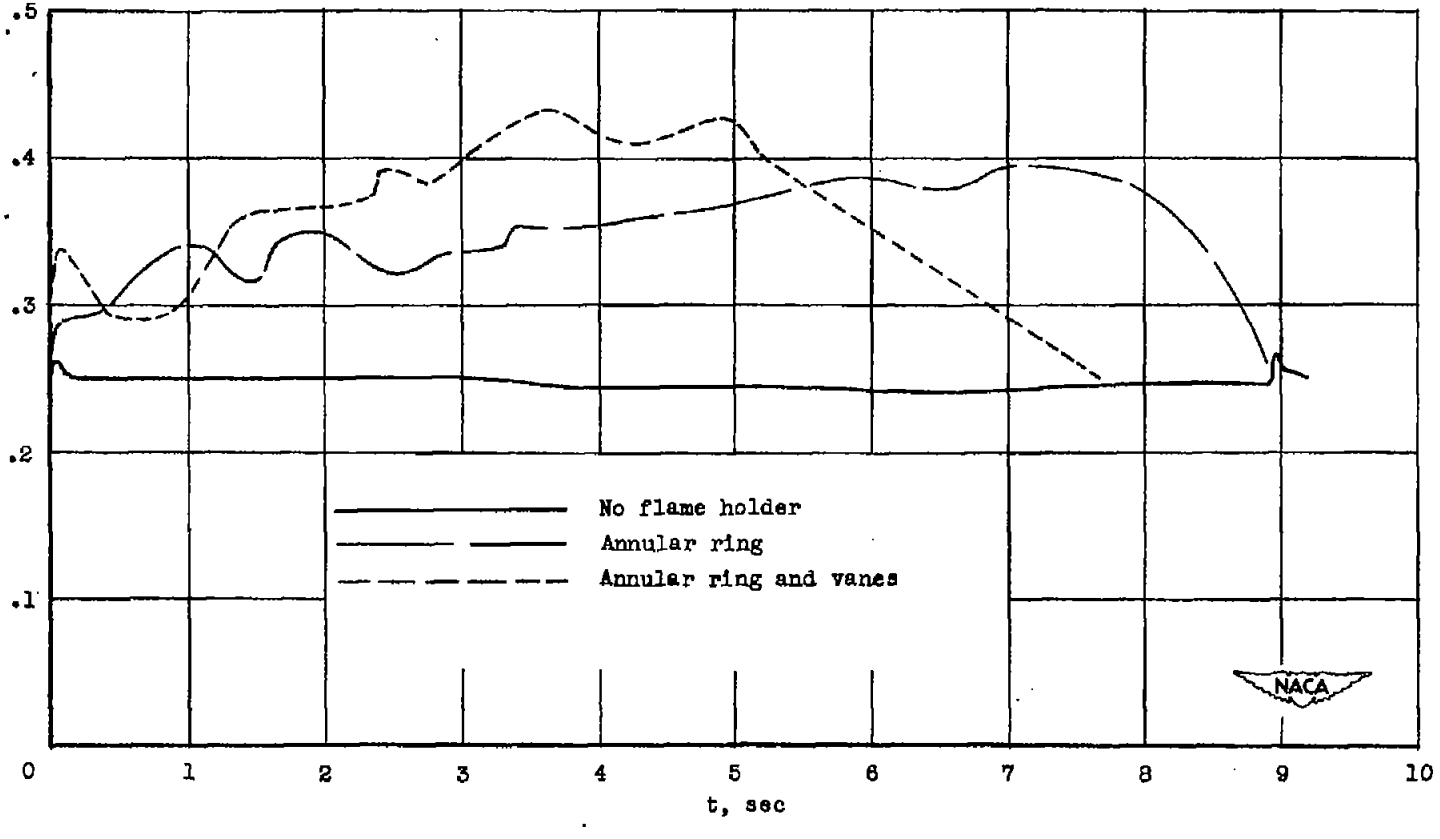

Figure 10.- Diffuser static pressure ratios against burning time for new-type end-burning fuels obtained in engine A, for different flame-holder configuration. M = 2.3; $W_a \approx 13.9$ pounds per second; $L^* = 43$ inches; $H_0 = 182 \pm 2$ psia.

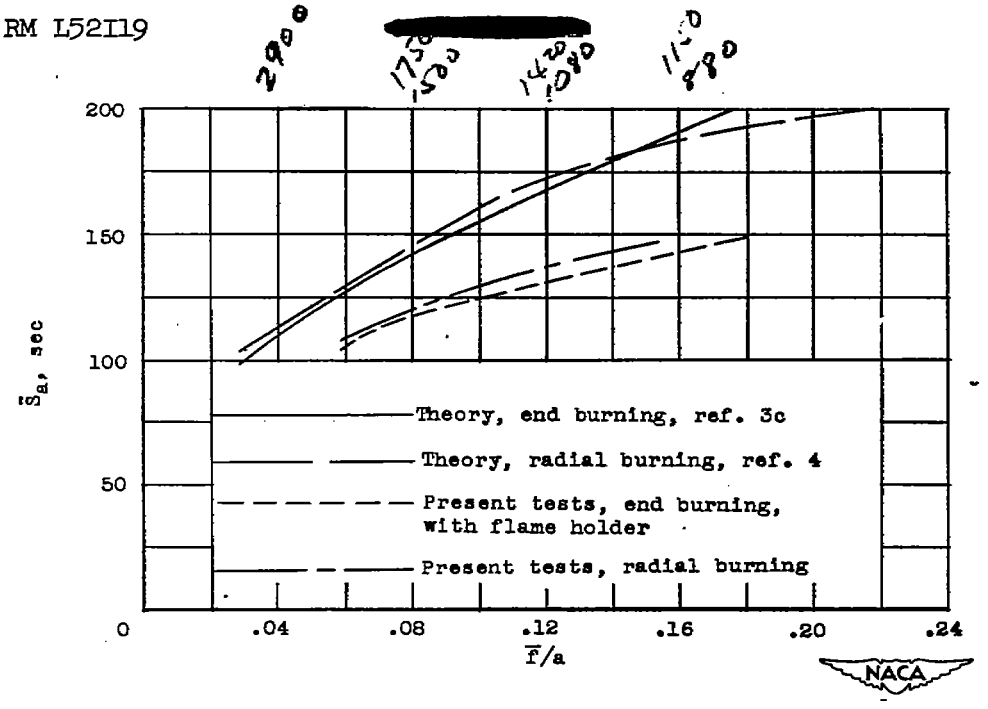

Figure 11.- Comparison of the average air specific impulses obtained with the new-type end-burning fuels with flame holders, and the radial-burning fuels with rubber-cement binder.

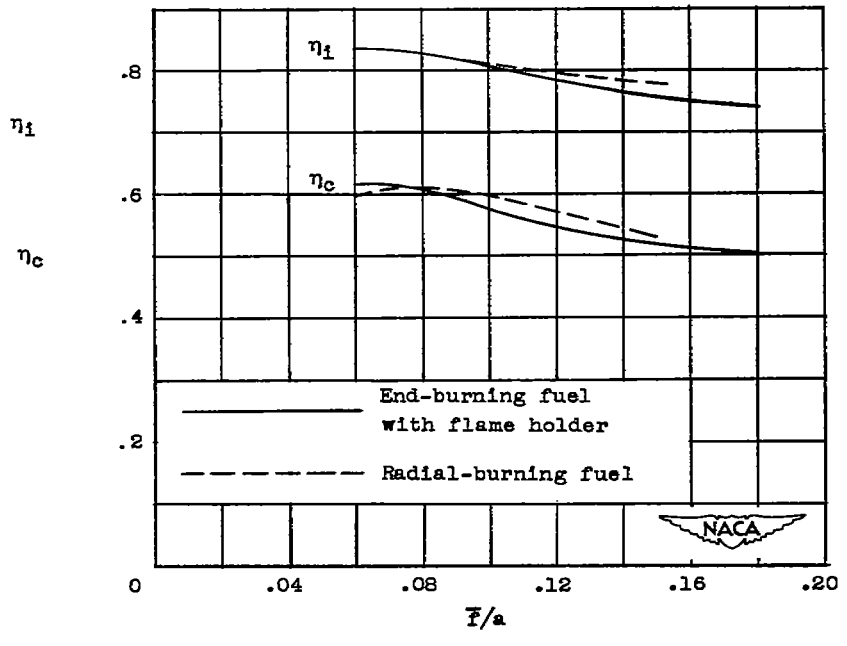

Figure 12.- Comparison of the impulse, η_i, and combustion, η_c, efficiencies obtained with the new-type end-burning fuels with flame holders, and the radial-burning fuel incorporating a rubber-cement binder.

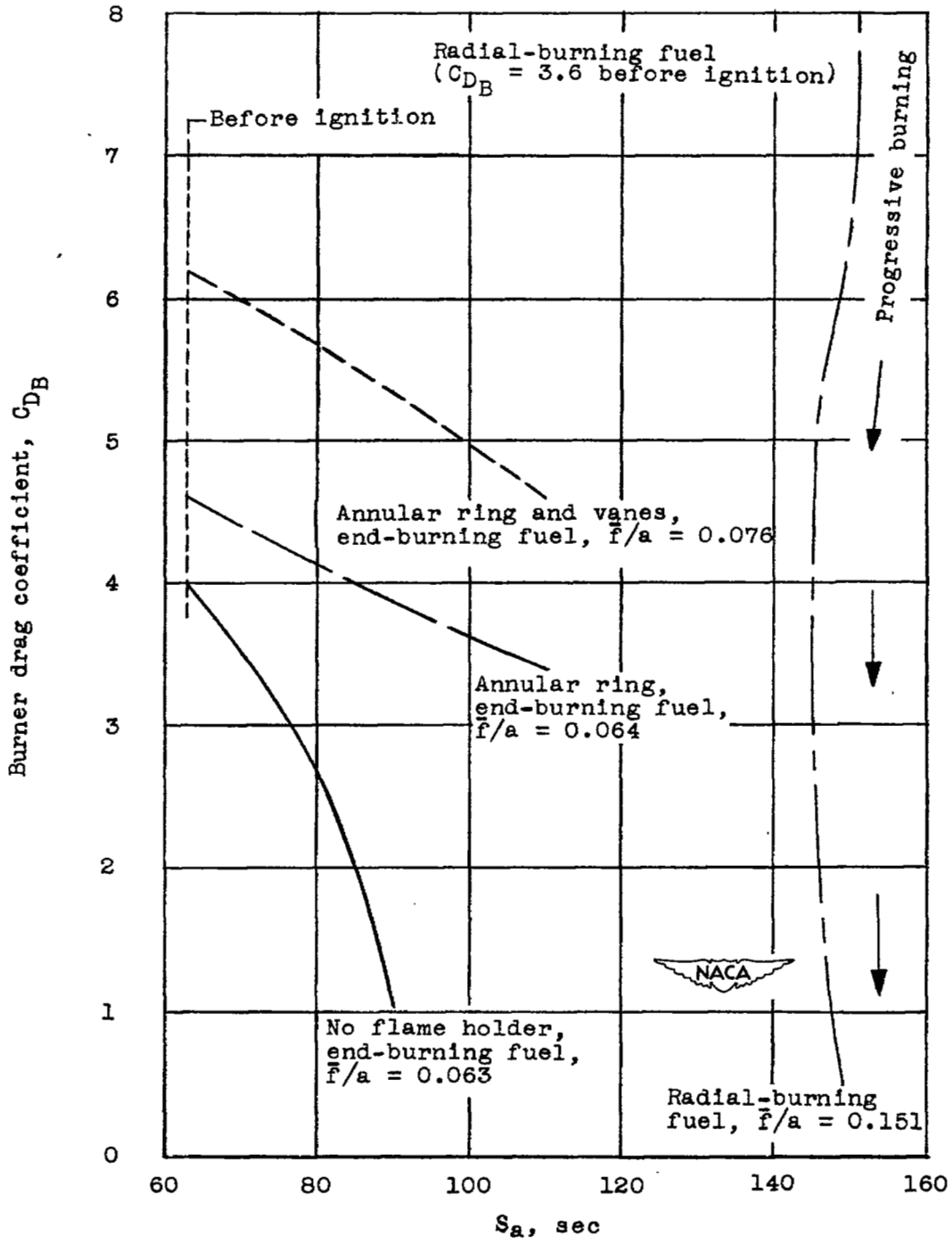

Figure 13.- Calculated values of burner drag coefficient, C_{D_B}, for the radial-burning fuel and for the end-burning fuel with various flame-holder configurations.